Introduction of Ag nanoparticles by picosecond LIFT to improve the photoelectric property of AZO films

Xiaofang Xu (许孝芳)[1,*], Jingbo Li (李精博)[1,], Xiaohan Yang (杨晓寒)[1], Sen Pan (潘 森)[1], and Yong Bi (毕 勇)[2]**

[1]*School of Mechanical Engineering, Jiangsu University, Zhenjiang 212013, China*
[2]*Nanjing Astronomical Instruments Co., Ltd., Chinese Academy of Sciences, Nanjing 210000, China*
**Corresponding author: xiaofangxu@aliyun.com; **corresponding author: 814687954@qq.com*
Received October 12, 2019; accepted December 19, 2019; posted online April 3, 2020

The photoelectric properties of conductive films are improved by doping Ag on aluminum-doped zinc oxide (AZO) films by laser induced forward transfer (LIFT). Firstly, the picosecond laser induced transfer mechanism of Ag films was revealed by numerical simulation; then, different-thickness Ag films were deposited on the AZO films by picosecond LIFT. When the film thickness is 30 nm and 50 nm, we have successfully obtained some Ag-AZO films with better optoelectronic properties by adjusting the laser parameters.

Keywords: LIFT; surface treatment; AZO film; Ag-nanoparticles; optoelectronic property.
doi: 10.3788/COL202018.043101.

Transparent conductive oxide (TCO) film is an important optoelectronic film with many characteristics including high conductivity, high absorption in the ultraviolet region, high transmission in the visible region, and high reflection in the infrared region[1]. Currently, it has been widely used in various fields such as photovoltaic cell components[2], touch panels[3], optoelectronic materials[4], liquid crystal displays[5], and gas sensors[6]. The aluminum-doped zinc oxide (AZO) film as one of the TCO films not only has good electrical conductivity and light transmission property, but also has the advantages of good thermal stability, abundant resources, and low cost. Therefore, it is widely used in the production of solar cells, liquid crystal display electrodes, and so on. With the increasing use of AZO films, their optoelectronic property demands are becoming higher and higher. As the optical transparency and electrical conductivity of the AZO films are contradictory and mutually constrained, it is necessary to control both of them in an optimum range to increase the conductivity while minimizing the decrease in transmittance.

The current researches for improving the optoelectronic property of AZO films mainly focus on two aspects. One way is to improve the preparation process of AZO films, including fabricating multilayer AZO, fluoride-doped tin oxide (FTO), and indium tin oxide (ITO) composite films, doping high-conductivity metal materials, and preparing thin metal layers to improve their comprehensive optoelectronic property[7,8]. Xu *et al.*[9] produced a mixed film of AZO/Ag nanowire (NW)/AZO sandwich structure by spin coating of Ag NWs. The Ag NWs were synthesized by the polyol method and inserted into the AZO layer, and the number of spin coating of Ag nanoparticles can change the optical properties and conductivity of the film. The thickness of the film is about 200 nm, the transmittance of the obtained film reached 80.5% at the 550 nm wavelength, and the sheet resistance reached 27.6 Ω/sq. The haze reached 14.9%. However, the method was complicated, the preparation of the film by the sol-gel method did not make it easy to control the uniformity of the film formation, and the preparation of the film with a relatively large thickness required a long experimental period. Xiong *et al.*[10] also used the sol-gel dip coating method to make an anti-reflection coating and obtained a thin film with a transmittance of 99.34% in the 450–950 nm band. The other way is to change the existing surface structure of the AZO films by micro-processing, including chemical etching[11], annealing[12,13], laser etching[14], surface texturing[15], etc. The surface of the film was treated to obtain a microporous or grid-like structure, which enhanced the scattering ability of incident light and improved its light transmittance. Inamdar *et al.*[16] used the wet chemical etching method with dilute hydrochloric acid to modify the AZO film. The optical properties of the film after etching were greatly enhanced, but the continuity of the film was destroyed, and the resistance value became large. Another problem is that the experimenter could not easily control the corrosion rate and corrosion depth with this method.

Laser induced forward transfer (LIFT) is a new manufacturing technology developed in recent years. It can rapidly deposit specific micro-patterns or microstructures on solid surfaces; therefore, it has a good development prospect in the field of micro–nano fabrication, especially the preparation of micro-optical devices[17]. For this reason, we applied this technology to the modification of transparent conductive films innovatively, that is, the highly conductive metal film was transferred by a picosecond laser to deposit metal nanoparticles with special optical properties on the surface of the AZO film; thereby, the sheet resistance of the AZO film would be reduced, and the quality factor of the transparent conductive film would be improved. The processing technology of the transparent conductive film can not only effectively improve the optoelectronic property of the AZO film, but also have

simple operation and easy control, and can be applied to micro-scale processing. This work can provide a new experimental basis for the application of the conductive film in the field of micro-machining.

In our work, we have simulated the laser ablated Ag film. In this study, we ignored the impact of laser scanning speed. When the picosecond laser irradiates on the metal film, there will be obvious non-equilibrium heat conduction between the electron and the lattice in the film. In addition, the spot size of the laser is much larger than the film thickness; therefore, the interaction between the picosecond laser and the metal film can be approximated by the nonlinear equation of the one-dimensional dual temperature model:

$$C_e\frac{\partial T_e}{\partial t}=\frac{\partial}{\partial x}\left(k_e\frac{\partial T_e}{\partial x}\right)-G(T_e-T_l)+S, \tag{1}$$

$$C_l\frac{\partial T_l}{\partial t}=\frac{\partial}{\partial x}\left(k_l\frac{\partial T_l}{\partial x}\right)+G(T_e-T_l), \tag{2}$$

where C represents heat capacity, T represents temperature, k represents the heat transfer coefficient, subscripts e and l represent the electrons and lattice, respectively, S is a laser heat source term, and G represents an electron-phonon coupling coefficient.

We use the finite element method to simulate the laser heating region, in which the laser heat source is expressed as follows due to the neglect of the spot size of the laser:

$$S=0.94\frac{(1-R)I}{t_p\alpha}\exp\left[-\frac{x}{\alpha}-2.77\left(\frac{t-t_p}{t_p}\right)^2\right], \tag{3}$$

where R is the laser reflectance of the metal film surface, $R=0.944$, I represents the absorbed laser energy density, t_p represents the duration of the laser pulse, i.e., the pulse width $t_p=10$ ps, and α represents the penetration depth of the laser, $\alpha=17.1$ nm.

The interaction between the picosecond single-pulse laser and the metal film was simulated by finite element analysis. The laser pulse width was set to 10 ps, the initial film temperature was 300 K, and, due to the short duration of the laser pulse, we ignored the heat conduction of the film and the constraining layer. The simulation results are as follows.

Figure 1 shows the change of lattice temperature in different-thickness Ag films irradiated by the picosecond laser with different energy densities, where the solid line represents the lattice temperature change of the rear surface of the Ag film, and the broken line represents the lattice temperature of the front surface of the Ag film (the direct irradiation surface of the laser). When different-thickness films are irradiated by a laser with the same energy density, as can be seen from Fig. 1 for the same film surface, the equilibrium lattice temperature of the Ag film decreases with the increase of the thickness of the Ag film. When the laser energy density is $0.2\,\mathrm{J/cm^2}$, the lattice temperature of the 30 nm Ag film reaches

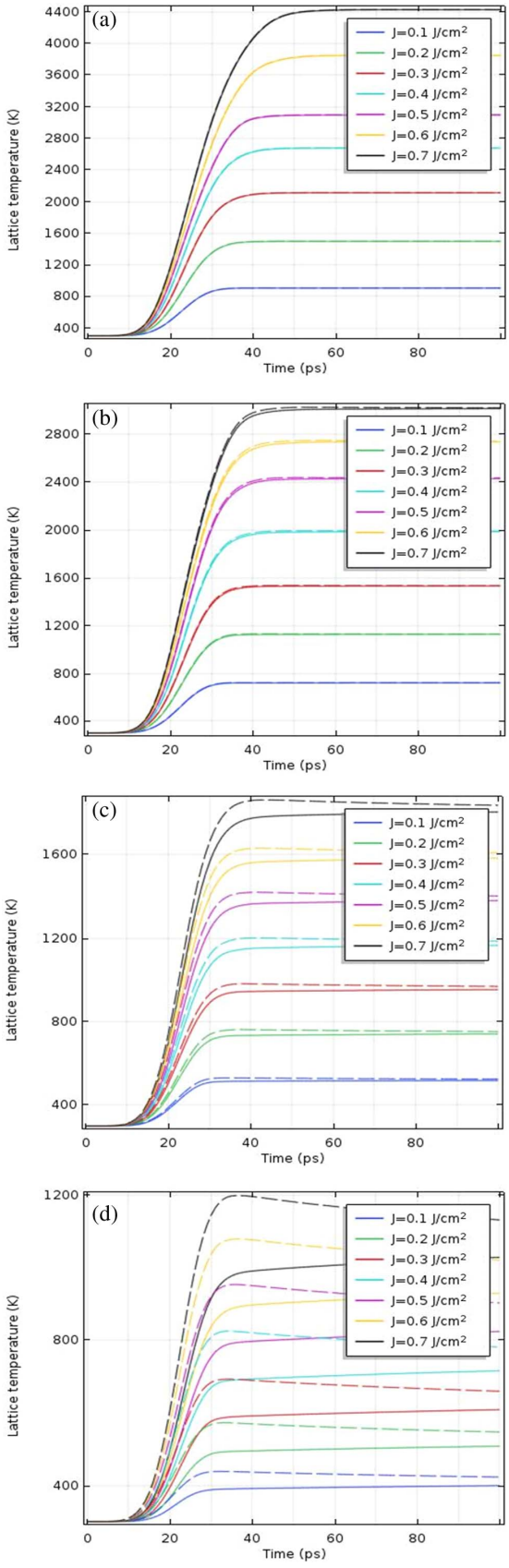

Fig. 1. Relationship between the lattice temperature of the Ag film and the picosecond laser energy density, wherein the thickness of the Ag film is (a) 30 nm, (b) 50 nm, (c) 100 nm, and (d) 200 nm.

the melting point, and the film will be melted; however, the surface temperatures of the 50 nm and 100 nm Ag films do not reach the melting point. When the laser energy density rises to 0.4 J/cm^2, the lattice temperature of the 30 nm Ag film is 2700 K and reaches the gasification temperature, so the whole film will be heated to the gasification state. But, the lattice temperature of the 50 nm Ag film only reaches the melting point, where the whole film is melted but is not gasified, and the surfaces of the 100 nm and 200 nm Ag films are still in a solid state.

In addition, as can be seen from Fig. 1, when the film thickness is small (such as 30 nm and 50 nm), the lattice temperatures of the front and back surfaces of the film are almost the same under the laser irradiating, and the film in the heated zone is completely heated instantly. We believe that when the film of smaller thickness (such as 30 nm and 50 nm) is transferred, the front and back surfaces of the film are simultaneously heated, and the heated region of the film will be simultaneously melted or vaporized to transfer so that metal nanoparticles are deposited on the receiving substrate. When the film thickness is gradually increased, the lattice temperature difference between the front and back surfaces of the film gradually increases [Figs. 1(c) and 1(d)]. When the laser energy density is 0.7 J/cm^2, the lattice temperature difference between the front and back surfaces of the 100 nm Ag film is about 100 K, and the lattice temperature difference between the front and back surfaces of the 200 nm Ag film is about 200 K. There is a possibility that the phase state of the front and back surfaces of the film is different, for example, the front surface has reached the melting temperature and is melted into a liquid state, but the back surface is still solid. For the same thickness of Ag film, when the laser energy density is gradually increased, the lattice temperature difference between the front and back surfaces is also gradually increased. As shown in Fig. 1(d), when the laser energy density is increased from 0.1 J/cm^2 to 0.7 J/cm^2, the lattice temperature difference between the front and back surfaces of the Ag film is gradually increased from 50 K to 200 K.

The simulation results show that the temperature difference between the front and back surfaces of different-thickness metal films has an effect on the film transfer mechanism. Therefore, the simulation results can help us quickly determine the threshold range of Ag film transfer during the experiment, which provides an important theoretical basis for the selection of experimental parameters.

Next, we conducted an experiment on film transfer. The LIFT experiment uses a multi-functional picosecond laser processing system, in which the picosecond laser has a center wavelength of 1064 nm, a pulse width of 10 ps, a maximum repetition frequency of 1000 kHz, and a beam quality factor of $M^2 \leq 1.5$. The schematic diagram of the system device is shown in Fig. 2. The spot radius at the focus is about 15 μm. The receiving substrate is placed in parallel under the transfer substrate, i.e., on the three-dimensional displacement platform, for receiving the deposited metal film. The distance between the film

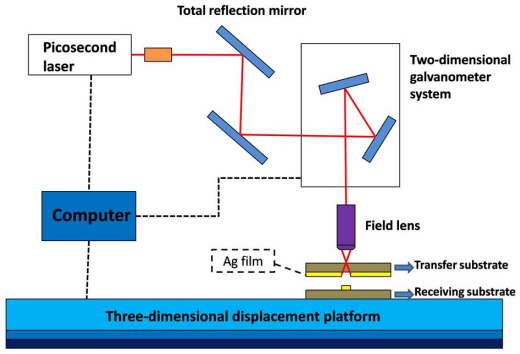

Fig. 2. Schematic diagram of the picosecond LIFT system.

layer and the laser focus is adjusted by controlling the three-dimensional displacement platform, and the control film layer is located at about 0.3 mm after the focus. The laser scanning adopts an "N"-shaped line scanning method to control the scanning pitch of $d \leq 30$ μm (Fig. 3), thereby achieving the maximum removal on the xy plane of the film. The scanning speed was adjusted to obtain a large area of deposited material on the substrate.

In this experiment, the receiving substrate was made of AZO film (commercial AZO glass) on a glass substrate, and the size is 15 mm × 15 mm × 2 mm. The average transmittance in the visible light band (380–780 nm) is 78%–82% measured by an ultraviolet-visible spectrophotometer. The sheet resistance of AZO films is between 8.9 Ω/sq and 9.5 Ω/sq measured by a four-probe sheet resistance meter, and the haze is low. Since Ag is the most conductive metal in nature, it is often used for doping various metal materials to improve its conductivity. Therefore, we used high-purity Ag (purity of 99.99%) as the doping metal and made some Ag films with thicknesses from 20 nm to 200 nm.

In this experiment, we deposited Ag nanoparticles on the AZO film by LIFT technology, which would change the conductivity and light transmittance of the AZO film, since the optoelectronic properties of the film are closely related to the film transmittance T_{av} (average transmittance of a film over a range of wavelengths) and the film sheet resistance R_s. In this experiment, we chose to measure the wavelength range from 380 nm to 780 nm and

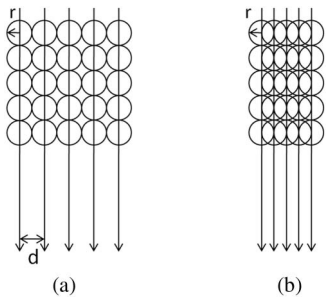

Fig. 3. Schematic diagram of laser scanning transfer processing. (a) Scanning pitch $d = 2r = 30$ μm. (b) Scanning pitch $d = r = 15$ μm.

Table 1. Experimental Parameters and Transmittance, Sheet Resistance, and Quality Factor of 50 nm Ag Film Transfer Sample

	Laser Parameter				
Number	E (J/cm^2)	V (mm/s)	T_{av} (%)	R_s (Ω/sq)	F_{TC} ($\times 10^{-2}$ Ω^{-1})
0	/	/	79.78	9.19	8.68
1	0.22	15	65.48	8.60	7.61
2	0.32	20	61.92	8.14	7.60
3	0.48	20	61.51	7.97	7.76
4	0.50	20	60.80	7.91	7.68
5	0.65	20	70.12	7.89	8.88
6	0.79	25	75.43	7.87	9.58
7	1.98	20	58.39	20.28	2.88

found the average transmittance T_{av}. The film quality factor F_{TC} is commonly used as a standard for measuring the integrated optoelectronic property of the film[18], $F_{TC} = T_{av}/R_s$; the higher the quality factor, the better the integrated optoelectronic property of the film.

Firstly, the transfer was carried out by using a 50 nm Ag film. Combined with the numerical simulation results of the previous section, the experimental parameters were continuously adjusted to obtain the optimized experimental results. The obtained experimental results are shown in Table 1. No. 0 is the original AZO glass sample. It can be seen that the sheet resistance of the receiving substrate of Nos. 1–6 is reduced compared with that of the sample of No. 0, and the average transmittance of the visible light band also decreases to some extent. It can be seen that when the laser energy density increases from 0.22 J/cm^2 to 0.50 J/cm^2, the average visible light transmittance decreases continuously; when the laser energy density increases from 0.22 J/cm^2 to 0.79 J/cm^2, the sample sheet resistance value also follows by falling. It is worth noting that the film quality factor of the No. 5 sample is 8.88×10^{-2} Ω^{-1}, and that of the No. 6 sample is 9.58×10^{-2} Ω^{-1}, which are both improved compared with 8.68×10^{-2} Ω^{-1} of the No. 0 sample. The integrated optoelectronic property of the film is improved. Surface morphology analysis for sample No. 6 is shown in Fig. 4, and the sectional view of Ag-AZO films is shown in Fig. 5.

From Figs. 4(a) and 4(b), we can also clearly see the deposition marks obtained on the AZO film after laser scanning of the Ag film, that is, the regional transfer of the metal film material is successfully realized by the LIFT method. The middle part between the straight lines in Figs. 4(a) and 4(b) is the laser scanning interval. In the laser central heating region, the Ag film deposition is less, and the deposition on both sides is more. This is consistent with the phenomenon that Jia *et al.* observed in the experiment of preparing nanostructured thin films by copper membrane transfer with more on both sides and less in the middle[19]. Further increasing the SEM magnification,

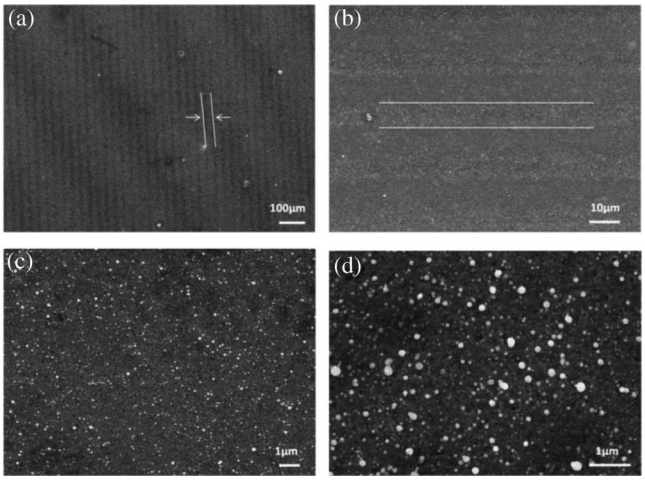

Fig. 4. Micro-morphology of AZO thin film after the transfer of 50 nm Ag film under parameters $E = 0.79$ J/cm^2, $v = 25$ mm/s: (a) 110 times, (b) 1000 times, (c) 5000 times, and (d) 17,000 times.

as shown in Figs. 4(c) and 4(d), we can see that a large number of white nanoparticles are scattered on the surface of AZO film. The energy spectrum analysis shows that the white particle component is Ag, and Ag particles are basically spherical and have a diameter ranging from 50 nm to 400 nm. Similarly, the nanostructures on the white AZO film shown in Fig. 5 are also Ag. By statistical analysis, we find that about 10% of the particles are between 300 nm and 400 nm, and about 80% of the particles are between 50 nm and 300 nm. These Ag nanoparticles independently exist but do not form a cluster structure. Since the Ag particles were introduced on the AZO film, the conductivity of the film is improved, but due to the obvious gap between the particles, the continuous metal film is not formed completely, and therefore, the improvement of electrical conductivity is not too great.

The mechanisms of laser ablation of the Ag film material and its transfer are very complicated. It can be

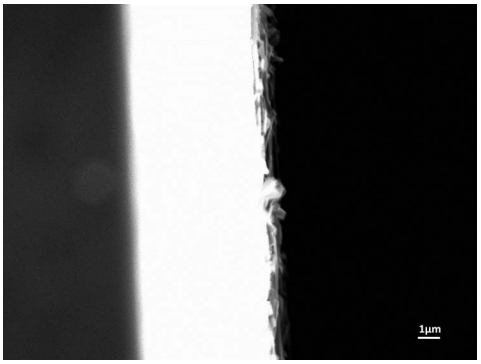

Fig. 5. Sectional view of Ag-AZO films after the transfer of 50 nm Ag film under parameters $E = 0.79$ J/cm^2, $v = 25$ mm/s.

known by theoretical simulation that when the Ag film is thin, the front and back surface temperatures of the film are almost the same, that is, the parts of the Ag film can be regarded as being simultaneously heated to the same temperature. When the laser energy is lower and below the ablation threshold of the Ag (the ablation threshold here is defined as the laser energy density at which the film material begins to undergo a phase change and melt), the Ag film is heated but does not undergo a phase change, and the temperature rise inside the film is insufficient to cause the film to fall off the substrate. When the energy gradually increases and is above the ablation threshold, the Ag film has reached the melting temperature at this point but has not yet reached the gasification temperature. Such as in samples Nos. 1–4, the laser energy density is 0.22 J/cm^2, 0.32 J/cm^2, 0.48 J/cm^2, and 0.50 J/cm^2, the material absorbs the laser energy and can rapidly be heated up, and the Ag film becomes molten and undergoes a phase change explosion that generates a certain driving force. At the same time, due to the small surface tension of the superheated liquid metal, the Ag film is deposited in a liquid form, and the cooling cladding and recrystallization of the droplet-like Ag on the receiving surface cause the light transmission property of the

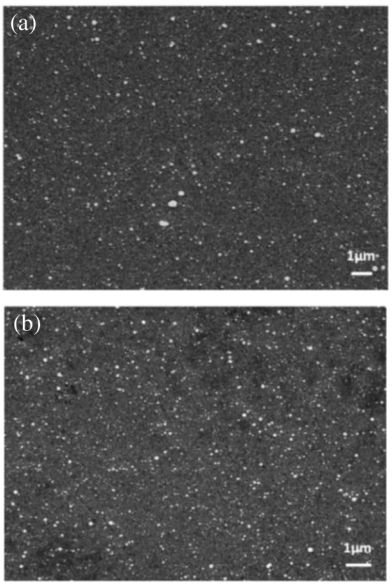

Fig. 6. (a) Micro-morphology of AZO film after the transfer of a 30 nm Ag film under parameters $E = 0.32$ J/cm^2, $v = 15$ mm/s; (b) micro-morphology of AZO thin film after the transfer of a 50 nm Ag film under parameters $E = 0.79$ J/cm^2, $v = 25$ mm/s.

AZO film at the receiving end to decrease. When the laser energy density is higher than 0.55 J/cm^2 [see Fig. 1(b)], the Ag film temperature will be higher than the gasification temperature. For example, in sample No. 6, the laser energy density is 0.79 J/cm^2, and the film temperature rapidly rises to a gasification temperature of 2485 K or higher. At this time, the entire Ag film is vaporized. Due to the gas phase expansion, the transfer of the film material is directly carried out in a sprayed manner or in a plasma state, and Ag is scattered into nanoparticles and emitted to the receiving substrate to cool the crystal. Since the Ag particle deposition is not transferred in liquid form at this time, the light transmission property of the AZO film is not greatly reduced. Next, a 30 nm Ag film is used for the transfer experiment, and the experimental

Table 2. Experimental Parameters and Transmittance, Sheet Resistance, and Quality Factor of 30 nm Ag Film Transfer Sample

	Laser Parameter				
Number	E (J/cm^2)	V (mm/s)	T_{av} (%)	R_s (Ω/sq)	F_{TC} ($\times 10^{-2}\,\Omega^{-1}$)
0	/	/	78.03	9.11	8.56
1	0.15	15	74.48	8.45	8.81
2	0.22	15	71.64	8.42	8.51
3	0.22	15	74.69	7.93	9.41
4	0.32	15	68.32	7.91	8.63
5	0.32	15	69.18	8.10	8.54
6	0.41	15	70.63	8.01	8.82
7	0.41	15	69.19	7.85	8.81

results obtained are shown in Table 2, respectively. It can be seen from Table 2 that the sheet resistance values of samples Nos. 1 to 7 are smaller than that of the untreated sample No. 0, but the film transmittance is also lower than that of the untreated sample No. 0. The quality factors of samples Nos. 1, 3, 4, 6, and 7 are higher than the quality factor of the original No. 0 sample, so their integrated optoelectronic property has been improved. In addition, from Table 2, we also find that the comprehensive optoelectronic property of the No. 3 sample film is the best; the gas plasma jet transfer of the whole film at a proper energy density can obtain high-quality Ag-AZO film. In addition, we compare the scanning electron microscopy (SEM) images of the No. 4 sample in Table 1 [Fig. 6(b)] and the No. 3 sample in Table 2 [Fig. 6(a)]. It can be seen that the number of Ag nanoparticles in Fig. 6(a) is less than that in Fig. 6(b), and the particle size is generally smaller than that in Fig. 6(b) by statistical analyzing. Therefore, we believe that in all effective transfers, the thicker the film is, the larger the size is, and the more nanoparticles we can obtain.

It can be seen from Table 2 that even under the same laser parameters, there are differences in the properties of the samples obtained by the experiments, such as sample No. 2 and sample No. 3. It seems that there is a problem with repeatability. In fact, in our experiments, we did find that its repeatability is not as good as other types of experiments. Limited by experimental conditions and complex transfer mechanisms, errors in the experiment occur. However, through a lot of experiments, we have gotten improved samples and found the correct experimental rules, achieving similar results, such as samples Nos. 4, 5 and samples Nos. 6, 7.

Table 3 and Fig. 7 show the surface roughness values and atomic force microscopy (AFM) images of the Ag-AZO film after the 30 nm Ag film was transferred. The No. 0 sample is an untreated AZO film with a surface roughness of 3.649 nm, as shown in Fig. 7(a). It can be found that the surface roughness of the AZO films was greatly increased after the transfer of the Ag film compared to the untreated sample. From Fig. 7(b) we can also see that some particles appeared on the surface of the Ag-AZO film, and the original film surface was not damaged.

Besides, we analyze some of the spectra of experimental samples obtained by the 50 nm and 30 nm Ag film transfers, as shown in Fig. 8. The curve of No. 0 is the spectral response curve of the original AZO film, and the transmittance curves correspond to the samples in Tables 1 and 2, where the curve numbers represent sample numbers, respectively. In addition to the ablation damage of the

Table 3. Surface Roughness of AZO Film after 30 nm Ag Film Transfer

Number	0	1	2	3
Roughness (nm)	3.649	17.596	20.367	21.485

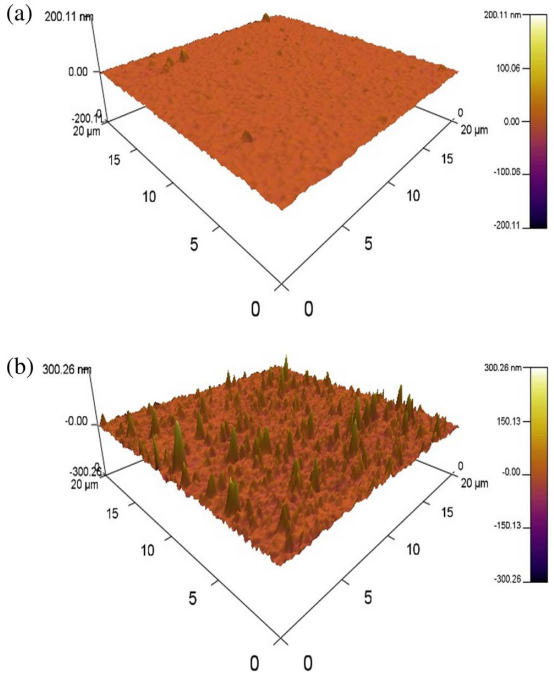

Fig. 7. (a) AFM diagram of initial AZO film; (b) AFM diagram of 30 nm Ag-AZO film.

AZO film caused by the high-energy laser irradiation in sample No. 7 in Table 1, the light transmittance of the sample is greatly reduced, resulting in different transmittance curves of other samples. The curves of the light

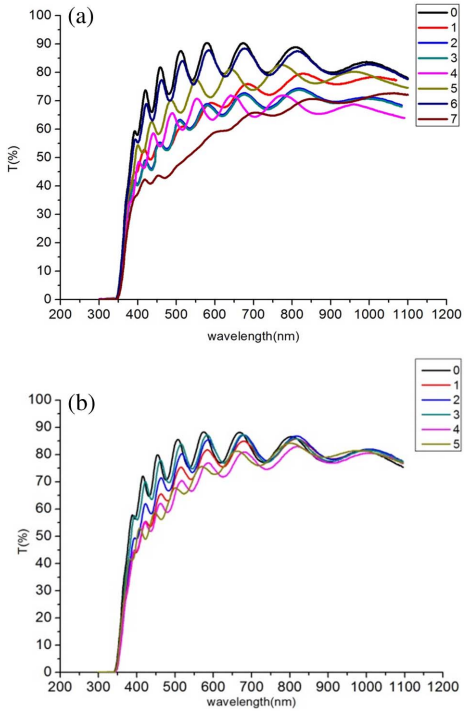

Fig. 8. (a) Light transmittance curves of the AZO film samples after the transfer of 50 nm Ag films; (b) light transmittance curves of the AZO film samples after the transfer of 30 nm Ag films.

transmittance of other samples in the 300–1100 nm band are basically the same as the curve of No. 0 sample and only decrease in value. This also excludes the effect of the introduced silver nanoparticles on the unique absorption of light in a certain band.

In conclusion, a method for improving the photoelectric characteristics of a transparent conductive film by LIFT of an Ag thin film is effective. When the film thickness is 30 nm and 50 nm, respectively, the AZO films with improved quality factor are successfully obtained by controlling the laser parameters. The quality factors are $9.58 \times 10^{-2}\ \Omega^{-1}$, $8.81 \times 10^{-2}\ \Omega^{-1}$, $9.41 \times 10^{-2}\ \Omega^{-1}$, and $8.63 \times 10^{-2}\ \Omega^{-1}$, which are higher than the quality factor of the original AZO film, so the feasibility of this LIFT scheme is verified. In addition, the finite element analysis method is used to simulate the thermal behavior of the metal film under the action of the picosecond laser. The lattice temperature changes of the front and back surfaces of the film with different film thicknesses and laser energy densities are obtained. When the film thickness is small ($\leq$100 nm), the forward transfer of Ag films occurs simultaneously in the whole heated region. This conclusion is used to guide the analysis of the experiment. This method can make transparent conductive films with high optoelectronic property relatively easily and has wide application prospects in micro–nano scale processing.

This work was partially supported by the Jiangsu Government Scholarship for Overseas Studies (No. JS-2018-253), the Jiangsu Natural Science Foundation Youth Fund (No. BK20150529), and the National Science Foundation for Post-doctoral Scientists of China (No. 2015M571678). The authors also acknowledge the teachers and students from the Institute of Surface and Interface Science in Jiangsu University for their guidance and help in the experiment.

References

1. L. J. Huang, N. F. Ren, B. J. Li, and M. Zhou, Mater. Lett. **116**, 405 (2014).
2. J. C. Bernède, L. Cattin, M. Morsli, and Y. Berredjem, Sol. Energy Mater. Sol. Cells **92**, 1508 (2008).
3. R. K. Gupta, K. Ghosh, R. Patel, S. R. Mishra, and P. K. Kahol, Mater. Lett. **62**, 4103 (2008).
4. H. Liu, V. Avrutin, N. Izyumskaya, Ü. Özgür, and H. Morkoc, Superlattices Microstruct. **48**, 458 (2010).
5. D. P. Puzzo, M. G. Helander, G. P. O'Brien, Z. Wang, N. Soheilnia, N. Kherani, Z. Lu, and G. A. Ozin, Nano Lett. **11**, 1457 (2011).
6. Y. S. Shim, H. G. Moon, D. H. Kim, H. W. Jang, C. Y. Kang, and Y. S. Yoon, Sens. Actuat. B **160**, 357 (2011).
7. N. F. Ren, L. J. Huang, M. Zhou, and B. J. Li, Ceram. Int. **40**, 8693 (2014).
8. T. C. Lin, W. C. Huang, and F. C. Tsai, J. Mater. Sci. – Mater. Electron. **26**, 3685 (2015).
9. Q. S. Xu, W. F. Shen, Q. J. Huang, and Y. Yang, J. Mater. Chem. C **2**, 3750 (2014).
10. H. Xiong, Y. X. Tang, L. L. Hu, and H. Y. Li, Chin. Opt. Lett. **17**, 033101 (2019).
11. S. H. Kim, D. J. You, J. H. Park, S. E. Lee, H. M. Lee, and D. Kim, Jpn. J. Appl. Phys. **51**, 10NB12 (2012).
12. L. J. Huang, B. J. Li, H. D. Cao, W. Zu, N. F. Ren, and H. Ding, J. Mater. Sci. – Mater. Electron. **28**, 4706 (2017).
13. J. N. Dong, J. Fan, S. D. Mao, Y. P. Lan, Y. G. Zou, H. Z. Wang, J. B. Zhang, and X. H. Ma, Chin. Opt. Lett. **17**, 113101 (2019).
14. W. M. Tsang, F. L. Wong, M. K. Fung, J. C. Chang, C. S. Lee, and S. T. Lee, Thin Solid Films **517**, 891 (2008).
15. X. Yan, S. Venkataraj, and A. G. Aberle, Energy Procedia. **33**, 157 (2013).
16. D. Inamdar, C. Agashe, P. Kadam, and S. Mahamuni, Thin Solid Films **520**, 3871 (2012).
17. P. Delaporte and A. P. Alloncle, Opt. Laser Technol. **78**, 33 (2016).
18. G. Haacke, J. Appl. Phys. **47**, 4086 (1976).
19. Y. Jia, S. T. He, H. Y. Song, Q. Y. Wang, and M. L. Hu, Chin. J. Lasers **44**, 0102009 (2017).